J. Biochem. 2009;146(1)61–70
doi:10.1093/jb/mvp047

Crystallographic Snapshots of an Entire Reaction Cycle for a Retaining Xylanase from *Streptomyces olivaceoviridis* E-86

Ryuichiro Suzuki[1,2], Zui Fujimoto[2], Shigeyasu Ito[1], Shun-Ichi Kawahara[3,*], Satoshi Kaneko[4], Kazunari Taira[3,5,6,7], Tsunemi Hasegawa[1] and Atsushi Kuno[8,†]

[1]Department of Material and Biological Chemistry, Faculty of Science, Yamagata University, Yamagata 990-8560; [2]Protein Research Unit, National Institute of Agrobiological Sciences, Tsukuba 305-8602; [3]Gene Function Research Center, National Institute of Advanced Industrial Science and Technology (AIST), Tsukuba 305-8562; [4] Food Biotechnology Division, National Food Research Institute, Tsukuba 305-8642; [5]Department of Chemistry and Biotechnology, School of Engineering, University of Tokyo, Tokyo 113-8656; [6]Tokyo University and Graduate School of Social Welfare, Isesaki, Gunma 372-0831; [7]Nagase & Co., Ltd, Nihonbashi, Tokyo 103-8355; and [8]Research Center for Medical Glycoscience, National Institute of Advanced Industrial Science and Technology (AIST), Tsukuba 305-8568, Japan

Received December 7, 2008; accepted February 28, 2009; published online March 11, 2009

Retaining glycosyl hydrolases, which catalyse both glycosylation and deglycosylation in a concerted manner, are the most abundant hydrolases. To date, their visualization has tended to be focused on glycosylation because glycosylation reactions can be visualized by inactivating deglycosylation step and/or using substrate analogues to isolate covalent intermediates. Furthermore, during structural analyses of glycosyl hydrolases with hydrolytic reaction products by the conventional soaking method, mutarotation of an anomeric carbon in the reaction products promptly and certainly occurs. This undesirable structural alteration hinders visualization of the second step in the reaction. Here, we investigated X-ray crystallographic visualization as a possible method for visualizing the conformational itinerary of a retaining xylanase from *Streptomyces olivaceoviridis* E-86. To clearly define the stereochemistry at the anomeric carbon during the deglycosylation step, extraneous nucleophiles, such as azide, were adopted to substitute for the missing base catalyst in an appropriate mutant. The X-ray crystallographic visualization provided snapshots of the components of the entire reaction, including the E·S complex, the covalent intermediate, breakdown of the intermediate and the enzyme–product (E·P)complex.

Key words: chemical rescue, crystallographic visualization, molecular evolution, retaining GH10 β-xylanase, switching enzyme with azide.

Abbreviations: Cel5A, GH 5 cellulase from *Bacillus agaradhaerens*; BSUA, α-amylase from *Bacillus subtilis*; CGTase, cyclodextrin glycosyltransferase from *Bacillus circulans* strain 251; Cel12A, GH 12 cellulase from *Humicola grisea*; Cel7B, GH 7 cellulase from *Fusarium oxysporum*; DNP2Fcell, 2,4-dinitrophenyl 2-deoxy-2-fluoro-β-D-cellobioside; Thio-DP5, Methyl 4′,4″,4‴-*S*-trithio-α-cellotetraoside; SoXyn10A, GH10 xylanase from Streptomyces olivaceoviridis E-86; pNP-X2, p-Nitrophenyl-β-D-xylobioside; MU-X2, 4-methylumbelliferyl-β-D-xylobioside; X5, xylo-pentasaccharide; LBHB, low-barrier hydrogen bond; CEX, GH10 xylanase from Cellulomonas fimi; ESI-MS, electrospray ionization mass spectrometry.

Glycosyl hydrolases are among the most diverse and ubiquitous enzymes involved in carbohydrate metabolism. They have recently been classified into approximately 100 families on the basis of similarities among deduced amino acid sequences (*1*). On the basis of their reaction mechanisms, glycosyl hydrolases are mostly classified as retaining or inverting enzymes because hydrolysis by these enzymes occurs with net retention (with double inversion) or inversion of the anomeric configuration, respectively (*2*). Since Koshland (*3*) first pointed out these two types of reaction mechanisms, many biochemical and structural studies have been carried out with the aim of confirming the details of these reactions (Fig. 1A). Although attempts have been made to visualize sugar-cleavage reactions by X-ray crystallography, beginning with studies on hen egg-white lysozyme (*4*), using substrate analogues and/or inactive mutated enzymes with recent technical advances in X-ray crystallography (*4–13*), structural analyses have been hampered by the unstable nature of the reaction intermediates. In 1988, a breakthrough was made by Withers and collaborators (*14*). They created a mechanism-based inhibitor that possessed both a good leaving group, such as a 2,4-dinitrophenyl moiety, and a 2-fluoride substitution in the sugar moiety located at the −1 subsite, and inhibited subsequent deglycosylation of the intermediate (*14–16*). As a result, a stable glycosyl-enzyme intermediate (E–I) was reliably formed. Since the Michaelis complex (E·S) could be visualized by use of a mutant enzyme or lowering the pH of the reaction, the novel mechanism-based inhibitor made it possible to obtain snapshots of the first glycosylation step. As a consequence, the potential conformational itinerary of glycosidases has been reported using X-ray

*Deceased December 1, 2004.
†To whom correspondence should be addressed. Tel: +81-298613187, Fax: +81-298613125, E-mail: atsu-kuno@aist.go.jp

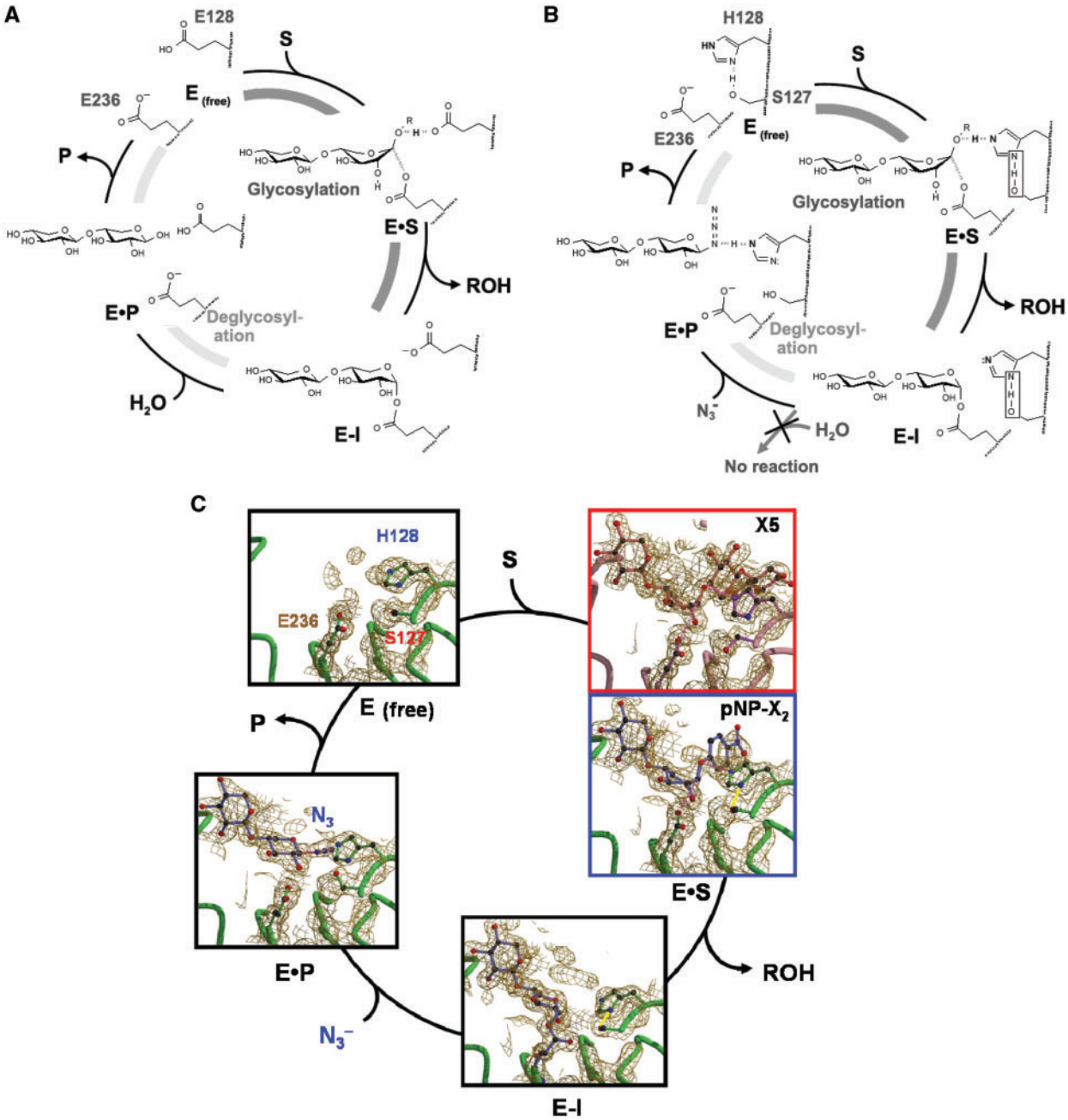

Fig. 1. **Complete mechanisms of reactions catalysed by wild-type SoXyn10A and SEA.** (A) Reaction cycle for wild-type SoXyn10A. (B) Reaction cycle for the SEA mutant. The LBHB-like interaction formed as part of the covalent intermediate is boxed. (C) Snapshots of the entire enzymatic reaction cycle catalysed by the SEA mutant. Key hydrogen-bonding interactions for the enzymatic reaction are indicated by dotted lines. The LBHB-like interaction formed as part of the covalent intermediate is indicated in yellow.

crystallographic or computational studies (*13*, *16–29*). However, from a different point of view, the stable E–I intermediate is totally resistant to subsequent deglycosylation and this prevents simultaneous visualization of the overall reaction cycle of the retaining enzyme. To overcome the problem associated with the stable E–I intermediate, we created a novel mutant, switching enzyme with azide (SEA), on the basis of the chemical rescue reaction (*30*, *31*) for xylanase SoXyn10A from *Streptomyces olivaceoviridis* E-86, a well-studied retaining enzyme (*32–40*). This mutant enzyme is active in the glycosylation step but inactive in the deglycosylation step in the absence of general nucleophiles. Structural analyses of the SEA allowed us to obtain snapshots of the components of the entire reaction, including the E•S complex, the covalent intermediate, breakdown of the intermediate and the enzyme–product (E•P) complex, of the xylanase simultaneously. Therefore, we were able to visualize the entire reaction cycle of this β-glycosidase, including the stereochemistry of the

nucleophilic attack on the anomeric carbon during the deglycosylation step.

MATERIALS AND METHODS

Error-Prone PCR and MU-Active Selection—The expression vector for the parent enzyme, pET28b(+)/E128H, was constructed as described previously (*33*, *35*). The open reading frame of E128H was amplified by error-prone PCR using the following primers: sense primer, 5′-TAA TAC GAC TCA CTA TA-3′; antisense primer, 5′-GCT AGT TAT TGC TCA GCG G-3′. The PCR product was purified using a Quantum Prep® Freeze 'N Squeeze DNA Gel Extraction Spin Column (Bio-Rad, Hercules, CA, USA). The resulting DNA fragment was digested with *Nco* I and *Hin*d III and ligated into the pET28b(+) vector to obtain randomized mutant libraries. Positive clones were selected from the mutant libraries on plates containing 4-methylumbelliferyl-β-D-xylobioside (MU-X_2) and 2.5 M sodium formate (*41*). The sequences of the positive clones were confirmed by nucleotide sequencing with an automated DNA sequencer (Model 310; PE Applied Biosystems, Foster City, CA, USA).

Saturation Mutagenesis—The N127 residue of SEA was randomized by saturation mutagenesis as described previously (*42*). Libraries were screened by assaying their catalytic activities toward MU-X_2 in the presence of 2.5 M sodium formate on plates (*41*). The sequences of the positive clones were confirmed by nucleotide sequencing as described above.

Enzyme Production and Purification—Overexpression in *Escherichia coli* and purification of the mutants, which were obtained by both random mutagenesis and saturation mutagenesis as described above, were performed as described previously (*33*). Every mutant was fused with a $(His)_6$-tag at the C-terminus for one-step affinity purification. After purification using a HiTrap chelating column (GE Healthcare, Buckinghamshire, UK), the resulting enzyme solution was desalted and concentrated to 1.0 mg/ml with a Microcon® YM-3 (Millipore Corporation, Bedford, MA, USA).

Characterization of Mutant Enzymes—The effects of sodium azide on the reaction rates of the mutants were determined as described previously (*33*). *p*-Nitrophenyl-β-D-xylobioside (pNP-X_2) was synthesized from a xylobiose, which was purified from a xylobiose mixture (Suntory Ltd, Osaka, Japan) as described previously (*43*). Enzyme reactions were performed under the following conditions. The reaction solution (45 μl) containing 0.5 mM pNP-X_2, 0.05% bovine serum albumin (BSA) and various concentrations of sodium azide (0–300 mM) in 25% McIlvaine buffer (a mixture of 0.1 M citric acid and 0.2 M Na_2HPO_4, pH 7.0) was preincubated at 30°C for 5 min. After the preincubation, 5 μl of enzyme solution (1.0 mg/ml) was added and incubated at 30°C for 1 h. Next, 50 μl of 0.2 M Na_2CO_3 was added to stop the enzyme reaction. The amount of *p*-nitrophenol released was determined by monitoring the absorbance at 400 nm using a spectrometer (DU 630; Beckman, Palo Alto, CA, USA).

Steady-State Kinetic Studies—The kinetic parameters of the mutants were determined as described previously (*33*). The final concentration of each mutant was 0.1 mg/ml. Various concentrations of the substrate in 25% McIlvaine buffer containing 0.05% BSA were preincubated at 30°C for 10 min before 50 μl of enzyme solution was added. The amount of *p*-nitrophenol released was determined as described above. For determinations of k_{cat} and K_M, the substrate concentrations were adjusted so that two sets of concentrations were above the estimated K_M, one was approximately equal to the estimated K_M and the other sets were below the estimated K_M.

Crystallographic Studies of SEA—The enzyme was crystallized by the hanging-drop vapor-diffusion method as described previously (*38*). Rod-like crystals of SEA ($0.6 \times 0.1 \times 0.1\,mm^3$) were obtained at room temperature from a protein solution (15 mg/ml) within 1 week. Crystals of the E•S complex, covalent E–I intermediate and hydrolytic product were prepared by soaking the crystals in a solution of pNP-X_2. Maps of the E•S complex were obtained after soaking the crystals in a solution of 4 mM substrate in 20% glycerol at acidic pH (pH 5.2) for 3 min. The covalent E–I intermediates were trapped by soaking the crystals in a solution of 4 mM substrate in 20% glycerol at pH 6.5 for 1 min. When the crystals were soaked in a solution of 4 mM substrate in 20% glycerol containing 2 M sodium azide at pH 6.5 for 1 min, maps of the product of azidolysis (β-xylobiosyl azide) in the catalytic cleft of SEA were obtained. All diffraction data were collected at beamline NW12 (Photon Factory, Advanced Ring (PF-AR), Tsukuba, Japan). The three types of crystals diffracted to resolutions of approximately 1.7 Å. The collected data sets were processed and scaled using the *DENZO* and *SCALEPACK* programs from the *HKL2000* package (Table 1) (*44*). All the SEA structures were determined by the molecular replacement method using the non-complexed SoXyn10A structure (PDB code: 1XYF) (*38*). The resultant F_{obs}–F_{calc} and $2F_{obs}$–F_{calc} maps yielded an electron density that corresponded to the soaked substrate. Though each crystal contained two molecules (A and B) in an asymmetric unit, we analysed a molecule A in detail. Manual model rebuilding was performed with the *QUANTA2000* program (Accerlys, San Diego, CA, USA). Models were refined by simulated annealing with the CNS program (*45*). The atomic coordinates and structure factors (PDB code 2D1Z, 2D20, 2D22, 2D23 and 2D24 for the Free SEA, E+S/pNP-X_2, EI/pNP-X_2, E+P/pNP-X_2 and E+S/X5, respectively) have been deposited in the Protein Data Bank, Japan, http://www.pdbj.org.

Mass-Spectrometric Analysis of Reaction Products—The reactions catalysed by wild-type SoXyn10A and SEA were subjected to electrospray ionization mass spectrometry (ESI–MS) for analysis of the reaction products generated with and without sodium azide. Mass spectra were acquired using an ion-trap spectrometer (ESQUIRE 3000; Bruker Daltonics, Bremen, Germany). The azide-rescue reaction was performed on a preparative scale to yield xylobiosyl azide as the major product as follows: A substrate solution (500 μl) containing 200 μg of pNP-X_2, 1 M sodium azide and 25% McIlvaine buffer was preincubated for 5 min at 30°C. After the preincubation, 50 μl of enzyme solution (0.1 mg/ml) was added to initiate the hydrolytic reaction, which was allowed to proceed for 2 h.

Table 1. **Summary of the data collection and refinement statistics.**

Data set	Free	E+S/pNP-X_2	EI/pNP-X_2	E+P/pNP-X_2	E+S/X_5
Data collection					
Space group			$P2_12_12_1$		
Unit cell (Å)					
a	78.51	78.47	78.69	78.93	75.70
b	94.06	94.11	93.96	94.09	94.09
c	139.66	139.86	139.72	139.47	138.37
Resolution (Å)[a]	50–1.60 (1.66–1.60)	50–1.85 (1.92–1.85)	50–1.70 (1.76–1.70)	50–1.95 (2.02–1.95)	50–1.85 (1.92–1.85)
Unique reflections	136,080 (13,147)	88,757 (8,780)	113,798 (11,132)	74,960 (6,547)	85,048 (8,396)
R_{merge} (%)[a]	4.4 (19.9)	5.1 (23.8)	4.1 (18.3)	7.4 (27.9)	6.7 (26.7)
Completeness (%)[a]	99.4 (97.1)	100 (100)	99.7 (98.8)	87.6 (86.6)	100 (100)
Average $I/\sigma(I)$[a]	31.8 (4.1)	39.6 (8.1)	48.5 (8.9)	20.8 (4.8)	35.7 (8.9)
Average redundancy[a]	6.8 (6.3)	7.4 (7.4)	6.5 (5.9)	3.0 (3.0)	7.4 (7.4)
Structure refinement					
Resolution range (Å)	47.03–1.60	44.60–1.85	32.21–1.70	47.05–1.95	36.51–1.85
No. of reflections	135993	88662	113707	66826	84968
R-factor (%)	19.1	18.1	18.6	18.3	17.7
R_{free}-factor (%)[b]	20.7	20.8	20.7	21.1	19.9
RMSD from ideal values					
Bond lengths (Å)	0.004	0.005	0.005	0.005	0.005
Bond angles (°)	1.30	1.30	1.30	1.30	1.30
Average *B*-factor (Å^2)					
Protein (chain A/B)	17.7/18.3	19.7/18.2	17.8/16.4	22.5/19.6	15.4/15.4
Water molecules	29.4	31.0	28.9	31.2	28.0
Sugars in chain A/B	–	43.1/38.4	13.9/9.4	31.6/22.7	28.0/28.3
Ramachandran plot (%)					
Favoured (chain A/B)	89.9/88.8	89.4/89.1	89.6/88.8	90.5/89.1	90.7/89.1
Allowed (chain A/B)	10.1/11.2	10.6/10.9	10.4/11.2	9.6/10.9	9.3/10.9
Disallowed (chain A/B)	0.0/0.0	0.0/0.0	0.0/0.0	0.0/0.0	0.0/0.0
PDB accession code	2D1Z	2D20	2D22	2D23	2D24

[a]Values for the highest resolution shell are given in parentheses. [b]The R_{free} factor is calculated using 5% of randomly chosen reflections.

RESULTS AND DISCUSSION

Creation and Characterization of a Switching Enzyme with Azide—To design our novel switching mutant xylanase, we reasoned that, as the replacement of a catalytic residue (E128) by a histidine residue inhibited the breakdown of the E–I intermediate (*33*), we might be able to restore the breakdown activity of the mutant by adding exogenous nucleophiles, such as sodium azide and sodium formate (Fig. 1B). We postulated that the resulting mutant may act as a 'switching enzyme with azide', abbreviated to 'SEA'.

Using error-prone PCR, we constructed the mutant by random mutagenesis from the almost inactive E128H mutant (Fig. 2; open circles) (*33*), which we chose as the parent enzyme. We obtained only one switching mutant, N127S-E128H (Fig. 2; closed circles), from 4,000 clones by active selection on MU-X_2 plates in the presence of sodium formate (MU-active selection). To clarify the importance of the effect of the N127 substitution with a Ser residue on the SEA activity enhanced by general nucleophiles, the N127 residue was randomized from the E128H mutant by saturation mutagenesis and screened. As a result of MU-active selection, two other positive clones, N127T-E128H and N127C-E128H, were selected

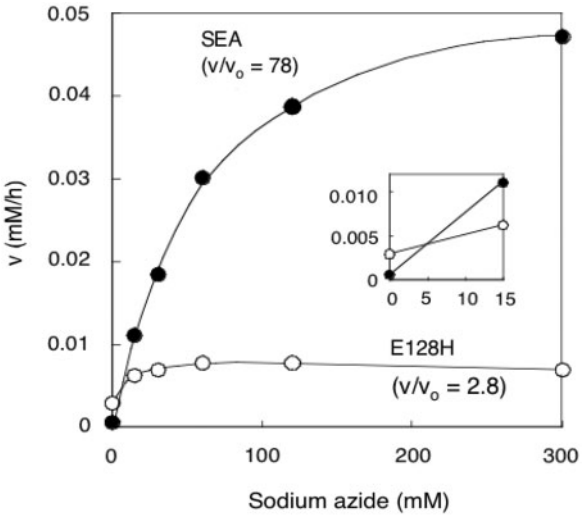

Fig. 2. **Chemical rescue by sodium azide of reactions catalysed by the SEA and E128H mutants.** The insert emphasizes the fact that the rate of hydrolysis of E–I by SEA (closed circles) is apparently zero in the absence of sodium azide, whereas the parental E128H (open circles) mutant has meaningful activity.

in addition to the N127S-E128H mutant. Note that all these N127 mutants are capable of maintaining hydrogen bonding interaction (see below for this interaction). Both of these selected mutants had significant but lower activities than N127S-E128H (Table 2). Therefore, we defined the most active N127S-E128H mutant as our SEA.

Next, the effects of a general nucleophile on the rate of hydrolysis by SEA were investigated. As shown in Fig. 2, the rate of hydrolysis by SEA was apparently zero in the absence of sodium azide. As a result, it was possible to accumulate the E–I intermediate. However, the breakdown rate of E–I was dramatically accelerated by two orders of magnitude in the presence of 300 mM sodium azide (Fig. 2). Under this condition, the k_{cat} value of SEA was about 10-fold higher than that of the parent enzyme E128H, while the second-order rate constant k_{cat}/K_M remained the same (Table 3).

The weak activity of SEA could also be enhanced by other nucleophiles (Table 4). The fact that the rate could be enhanced by the addition of nucleophiles indicates that the deglycosylation step, rather than the glycosylation step, is the rate-limiting step for these mutant enzymes (*46*).

In the overall transition state, the nucleophile attacks the anomeric carbon atom of the E–I intermediate in a concerted bimolecular S_N2 reaction, leading to the completion of the deglycosylation reaction (see below). On the other hand, no similar levels of acceleration by azide and carboxylate anions were observed with other acid/base-substituted mutants, such as E128H (Table 4), E128A and E128Q (data not shown) (*33*). The creation of SEA allowed us to control the breakdown of E–I using a general nucleophile, and we anticipated that it might allow us to obtain snapshots of the enzyme complex at each step in the reaction (Fig. 1B and C).

The Michaelis Complex with the Natural Substrate—Next, we examined whether and confirmed that snapshots of the reaction cycle of SEA could be obtained by X-ray crystallography (Fig. 1C and Supplementary Fig. S1). Under substrate-free conditions (E), the overall structure of SEA was similar to that of wild-type SoXyn10A except at the site of the substitution (PDB accession code: 2D1Z). When crystals of the enzyme were soaked in xylo-pentasaccharide (X5) as a substrate at low pH (pH 5.2) as described previously (*17*), the E•S complex was formed (Fig. 3 and Supplementary Fig. S1c). Based on the site designations in previous studies (*36*, *37*, *39*), the pentasaccharide appeared to lie at subsites –2 to +3 but there was no interaction at subsite +3. Figure 3 shows a visualization of the E•S complex with the intact and uncleaved β-linked glycoside within the enzyme, which contains both the proton donor and the nucleophile (*47*, *48*). The sugar moiety at subsite –1 formed a distorted $^1S_3$ skew-boat conformation (Fig. 4 and Supplementary Fig. S1c), which has been seen in E•S complexes within other retaining β-glycoside hydrolases acting on *gluco*-configured substrates (*17*, *23*, *25*, *48*, *49*).

As can be seen in Fig. 4A and B, the lone-paired electrons on the ring oxygen O-5 (indicated by *app*) were still antiperiplanar to the leaving oxygen for both the natural (X5) and pNP-X_2 substrates, in agreement with the anomeric effect in the ground state (*50*, *51*). However, the ring was distorted such that the stable oxocarbonium ion-like transition state could be achieved with minimum movement. As expected from the above considerations, residue H128 in the E•S complex

Table 2. **Comparison of the azidolysis rates of N127 substituents for pNP-X_2.**

Enzyme	Nucleophile	V (x10^3) (mM/hr)
N127S-E128H	Sodium azide	47
N127T-E128H	Sodium azide	13
N127C-E128H	Sodium azide	1.7

Table 3. **Kinetic parameters of SoXyn10A and its mutants for pNP-X_2 in the presence of sodium azide.**

Enzyme	k_{cat} (min^{-1})	K_M ($\times10^2$) (mM)	k_{cat}/K_M ($min^{-1}\,mM^{-1}$)
Wild-type	2,530 ± 3	237 ± 5	1,080 ± 3
E128H	0.31 ± 0.01	0.821 ± 0.04	37.8 ± 2.7
SEA	3.14 ± 0.3	7.89 ± 0.3	39.8 ± 1

Table 4. **Reaction rates of E128H and SEA in the presence of general nucleophiles.**

Enzyme	Nucleophile	V ($\times10^3$) (mM/h)	V/V_0
E128H	–	2.9	1.0
	Sodium azide	6.9	2.3
	Potassium thioacetate	5.6	1.9
	Sodium acetate	7.1	2.4
	Sodium formate	8.3	2.8
	Potassium fluoride	18	6.1
	Potassium chloride	4.5	1.5
	Potassium bromide	4.9	1.7
	Potassium iodide	4.1	1.4
SEA	–	0.59	1.0
	Sodium azide	47	78
	Potassium thioacetate	32	54
	Sodium acetate	26	44
	Sodium formate	19	32
	Potassium fluoride	2.8	4.6
	Potassium chloride	0.96	1.6
	Potassium bromide	1.3	2.1
	Potassium iodide	0.80	1.7

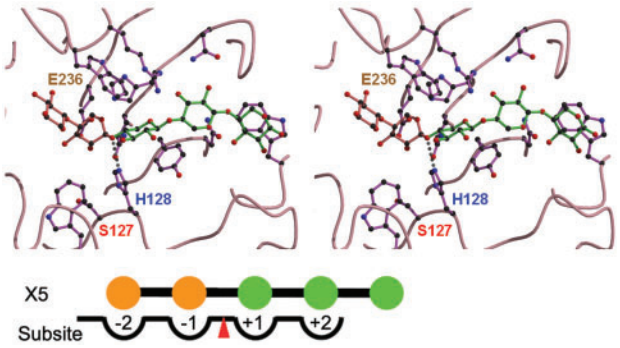

Fig. 3. **Stereoscopic overview of a schematic representation of the natural substrate (X5) bound at the active site of SEA.** Key hydrogen-bonding interactions for the enzymatic reaction are indicated by dotted lines.

remained at the appropriate position for its role as a proton donor (Fig. 4B) (*17*).

In general, a significant part of the binding energy in enzymatic reactions is utilized to provide the driving force for catalysis by causing localized destabilization, a conformational change (such as the creation of a distorted $^1S_3$ skew-boat conformation), more productive binding or greater loss of entropy in the E•S complex (*52*). As a result, the free energy of binding can be utilized to decrease the free energy of activation and bring about an increase in the reaction rate (*52*). In the present case of the first glycosylation step, distortion to yield the $^1S_3$ skew-boat conformation for activation of translating bonds and stabilization of the leaving O-1 oxygen by proton transfer should play a major role in catalysis. Notably, the hydrogen-bonding pattern observed with pNP-X_2 (Fig. 4A) was different from that observed with X5 (Fig. 4B). In the case of pNP-X_2, the lone-paired electrons on O-1 are sp^2 hybridized because they are conjugated with the aromatic ring, whereas the corresponding electrons of the natural leaving group are sp^3 hybridized. Indeed, the dihedral angles between the proton donor (H-Nε of H128) and the carbon of the leaving group were 91° and 113° for pNP-X_2 and X5, respectively, as shown at the top of Fig. 4A and B. Each dihedral angle was clearly consistent with those in other E•S complexes described previously (Table 5) (*12*, *17*, *23*, *47–49*).

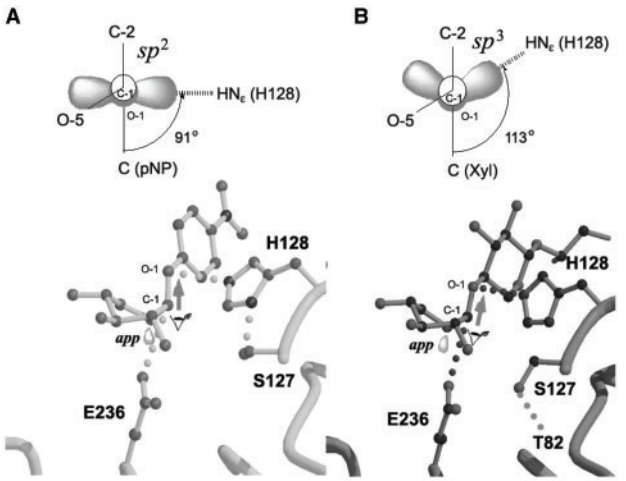

Fig. 4. **Structures of Michaelis complexes.** The structures of pNP-β-D-xylobioside (A) and the natural substrate (B) are shown for comparison. The configurations of the covalent and hydrogen bonds along C-1 and O-1 are shown at the top.

Moreover, the distance between Nε of H128 and O-1 was shorter for pNP-X_2 (3.0 Å) than for X5 (3.3 Å). Owing to these slight changes in the hydrogen-bonding patterns, the stable low-barrier hydrogen bond (LBHB)-like interaction (2.5 Å) between Nδ of H128 and Oγ of S127 in the SEA–pNP-X_2 complex was not maintained in the SEA–X5 complex (Fig. 4) (*53*, *54*). As a result, the Oγ of S127 swung away from H128 in the SEA–X5 complex (Fig. 4B) to participate in a new hydrogen-bonding interaction (2.9 Å) with Thr82. The sugar rings at subsites –1 and +1 in the SEA–X5 complex must have been fixed in the SEA–pNP-X_2 complex because of the interaction of subsite +2 with X5. Therefore, it is probable that the orientation and conformation of the SEA–X5 complex, visualized here using an active enzyme, are maintained in the wild-type xylanase.

Trapping the Covalent Glycosyl–Enzyme Intermediate—We obtained the structure of the covalent E–I intermediate by raising the pH of the E•S crystals to 6.5 (Fig. 5A and Supplementary Fig. S1d). The conformation of the sugar in the covalent intermediate was changed to a $^4C_1$ chair-form and was similar to that described in previous reports (Fig. 5) (*13*, *16–20*, *23*, *26*). We noted that S127 and H128 of SEA moved, as did the sugar moiety, without loss of the LBHB network (2.5 Å; Fig. 5A). As a result, Nε of H128 was no longer able to interact with the water molecule that is supposed to attack C-1 at the next deglycosylation reaction step. Therefore, E–I intermediates were easily accumulated when we used SEA, even when the non-fluoro compound pNP-X_2 was used as the substrate (Fig. 5).

In contrast, when we used the single mutant (E128H), the E–I intermediates failed to accumulate under similar conditions (data not shown). Previously, it was reported that the almost inactive double-mutant (DM) of the Cex

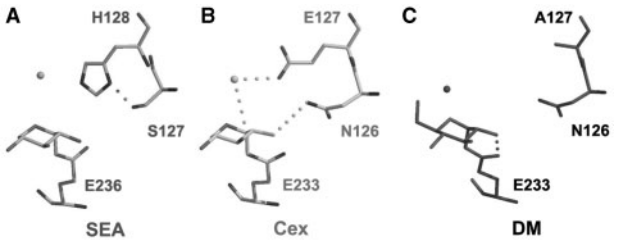

Fig. 5. **Differences among structures of covalent intermediates in reactions catalysed by SEA (A), wild-type Cex from *Cellulomonas fimi* (B; PDB accession code: 2XYL) and a DM mutant of Cex (C; PDB accession code: 2HIS).**

Table 5. **Comparison of the dihedral angles between the proton donor and the carbon of the leaving group.**

Enzyme	Substrate	Configuration	PDB code	Angle	Reference
SEA	pNP-X_2	$^1S_3$	2D20	91°	This work
Cel5A	DNP2Fcell	$^1S_3$	4A3H	88°	17
Cel5A	DNP2Fcell	$^1S_3$	1H2J	81°	23
SEA	Xylopentaose	$^1S_3$	2D24	113°	This work
BSUA	Maltopentaose	Deformed $^4C_1$	1BAG	110°	12
CGTase	Maltononaose	Deformed $^4C_1$	1CXK	111°	47
Cel12A	Cellopentaose	$^1S_3$	1UU6	118°	48
Cel7B	Thio-DP5	$^1S_3$	1OVW	121°	49

endo-glucanase/xylanase from *Cellulomonas fimi* formed an LBHB-type hydrogen bond (2.4 Å) between the O-2 of a non-fluoro substrate and the carbonyl oxygen of the nucleophile (E233), instead of the native hydrogen bond between N126 and O-2, which is believed to be the important hydrogen-bonding interaction for maintenance of an active intermediate (Fig. 5B and C) (*13*). In the case of SEA, N127 (corresponding to N126 in DM; Fig. 5C) was replaced by a Ser residue, with the resultant loss of the important hydrogen-bonding interaction with O-2, similar to the case for DM (Fig. 5). In fact, the single N127S substitution in wild-type SoXyn10A reduced the catalytic activity ($k_{cat} = 280\,min^{-1}$ and $K_M = 2.9\,mM$). Taken together, our results indicate that, when the enzyme is SEA, the breakdown of the E–I complex is interrupted by LBHB formation between S127 and H128 (2.5 Å), in association with the loss of the important hydrogen bond between N127 and O-2 that is likely to assist the cleavage of the glycosyl bond of E–I.

Visualization of the Deglycosylation Step—According to our scheme for the chemical rescue of the reaction catalysed by SEA, the deglycosylation reaction should start immediately upon the addition of sodium azide (Figs. 1B and 2). If the reaction proceeds cleanly, the exclusive product should be a xylobiosyl azide with a specific β-configuration. We tested this hypothesis by monitoring SEA-mediated cleavage in a solution of pNP-X_2 or X5 in the presence of azide. In reactions with either pNP-X_2 or X5, ESI–MS analyses demonstrated that only the expected xylobiosyl azide was obtained, without any contamination by the hydrolysis product, xylobioside (Fig. 6). To visualize and characterize the mechanism of SEA-catalysed deglycosylation, we soaked crystals of SEA plus substrate in a solution of sodium azide. X-ray crystallography revealed that the β-xylobiosyl azide was present in the E•P complex and the azide moiety with the expected β-configuration was trapped at the cleft at the +1 subsite (Fig. 7A and Supplementary Fig. S1e). The electron densities of both C-1 and azide were clearly recorded, whereas snapshots generally failed to locate the nucleophile and C-1 atom because mutarotation at C-1 appeared to have taken place and anomeric mixtures

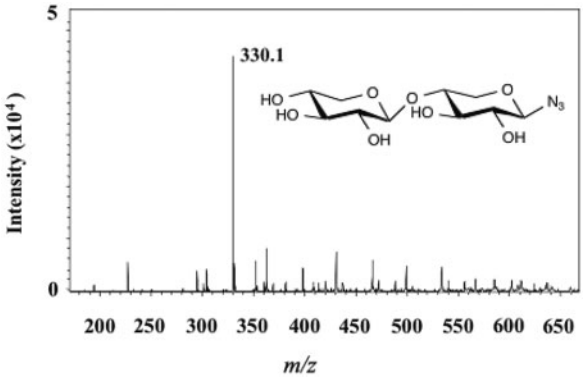

Fig. 6. **Identification of an enzymatic reaction product of SEA in the presence of sodium azide by ESI-MS.**

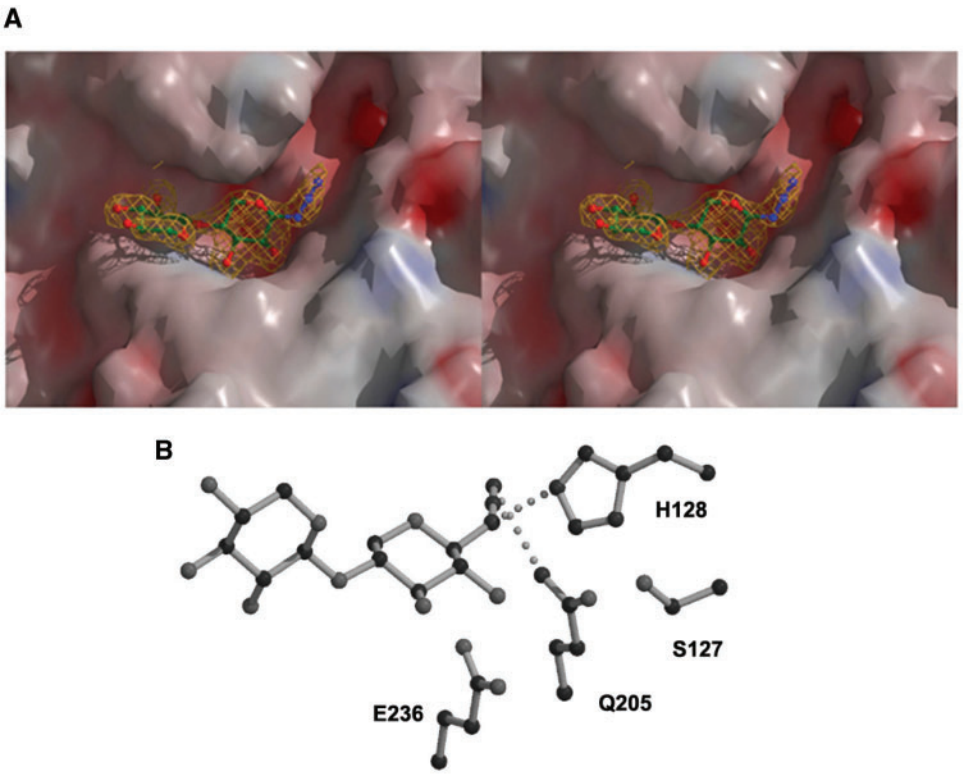

Fig. 7. **The second deglycosylation step.** (A) F_{obs}–F_{calc} omit electron-density maps of the reaction product, β-xylobiosyl azide, in a complex with SEA contoured at 3.5σ. The azide moiety in the product is indicated in blue. (B) Interaction of the β-xylobiosyl azide with SEA.

accumulated as E•P (*17*, *19*, *23*). We found that Nε of residue H128 interacted with N-1 of the azide moiety at a distance of 2.8 Å (Fig. 7B), while Nε of Q205 was close to N-2 and N-3 of the azide. In addition, the distance between S127 and H128 was increased to 3.3 Å and, as a result, the LBHB observed in E–I disappeared (Fig. 7B). Moreover, the C-1 atom, whose position controls the stereoelectronic effects of O-5, returned from the downward E–I position to the original position of C-1 in the E•S complex (Fig. 8). Accordingly, the stereoelectronically important O-5 atom jumped dramatically over a distance of 1.5 Å (Fig. 8A). This dramatic leap by an O-5 atom has not previously been reported.

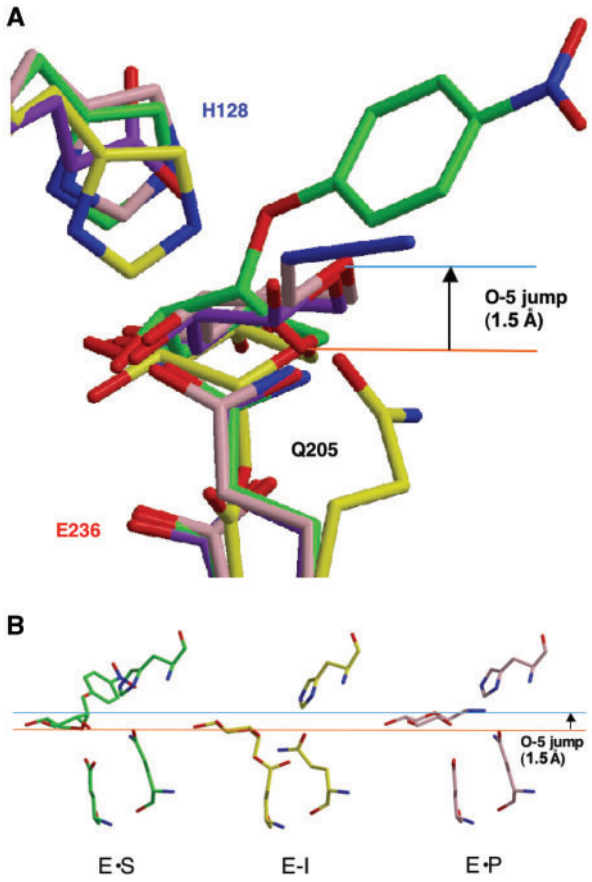

Fig. 8. **Superposition of the structures of the entire reaction.** End (A) and side (B) views of every reaction step for SEA. The Michaelis complex (green), covalent intermediate (yellow) and reaction product (pink) are shown. As a reference, the complex between SoXyn10A and the reaction product (PDB code: 1ISW) is indicated in purple.

Taking all our observations into account, we propose a reaction mechanism for the deglycosylation step of SEA (Fig. 9). Within E–I, Nε of H128 is not protonated and the LBHB between S127 and H128 inhibits the activation of the water molecule that is supposed to attack C-1 in the reaction catalysed by the wild-type enzyme. Within E–I, the lone-paired electrons on O-5 are antiperiplanar to the E236 oxygen. Applying the principle of microscopic reversibility, we propose that the antiperiplanar orbital at O-5 should facilitate both the cleavage of the oxygen–C-1 bond (Fig. 4) and the nucleophilic attack by the azide at C-1, as shown in parentheses in Fig. 9. Therefore, when reactive azide is added and attacks the C-1 atom, the sugar moiety at subsite -1 of the product is temporarily distorted to form the $^{1}S_{3}$ skew-boat conformation. After the decay of the intermediate, the sugar moiety moves back to the chair conformation as a result of the leap of the stereoelectronically pivotal O-5 atom over a distance of as much as 1.5 Å (Fig. 8). Finally, the product is released from the active site and the reaction can begin again (Fig. 1C).

Conclusions—In the present study, we have obtained a complete set of snapshots for the entire reaction catalysed by a retaining enzyme, the xylanase from *Streptomyces olivaceoviridis* E-86, using both xylooligosaccharides and more reactive substrates (Fig. 1C and Supplementary Fig. S1). Although every snapshot was obtained using crystals of a site-directed mutant, the conformational itinerary of the glycosylation step from the $^{4}C_{1}$ chair conformation to the $^{1}S_{3}$ skew-boat conformation is in agreement with previous observations (*17*, *23*, *25*, *28*). In addition, we have proposed a reaction mechanism through the $^{1}S_{3}$ conformation for the deglycosylation step by visualization of azidolysis by SEA.

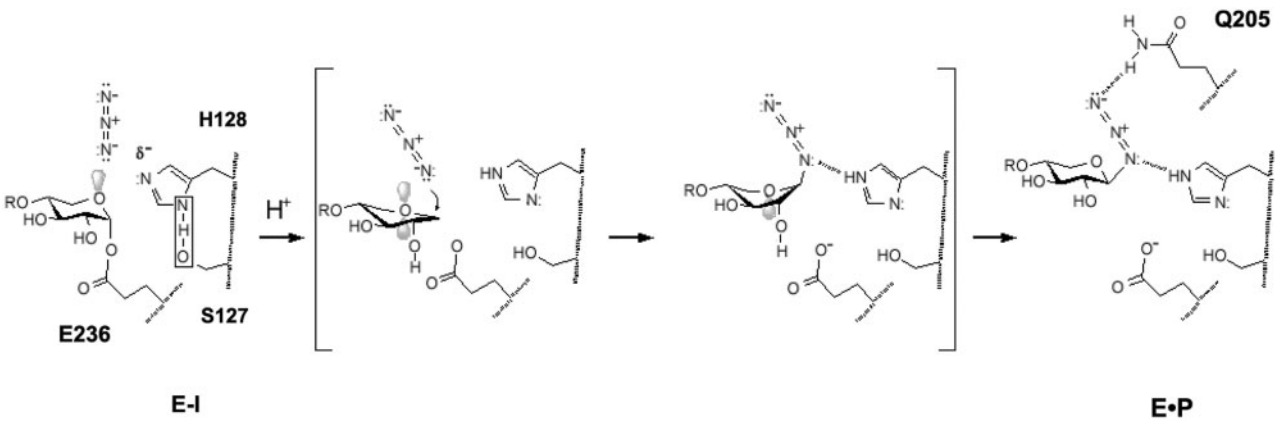

Fig. 9. **Hypothetical mechanism for the second deglycosylation step in the reaction catalysed by SEA.** Lone-paired electrons on the ring oxygen O-5 are indicated in gray.

Our achievements were based on successful selection of an active switching enzyme that we designated SEA. Both N127 and E128 are strongly conserved in the so-called clan A glycosyl hydrolases (*1*). Therefore, our present demonstration of a complete set of snapshots of an entire reaction may be of general significance and may also be applicable to related enzymatic reactions.

SUPPLEMENTARY DATA

Supplementary data are available at *JB* online.

ACKNOWLEDGEMENTS

The authors would like to thank Drs J. Hirabayashi and M. Momma for helpful comments, Mr. S.-N. Iwamatsu for assistance with biochemical experiments, and the beamline scientists at the Photon Factory in Tsukuba for assistance with the collection of X-ray data.

FUNDING

Program for the Promotion of Basic Research Activities for Innovative Bioscience (BRAIN); New Energy and Industrial Technology Development Organization (NEDO) in Japan.

CONFLICT OF INTEREST

None declared.

REFERENCES

1. Coutinho, P.M. and Henrissat, B. (1999) *Recent Advances in Carbohydrate Bioengineering*, pp. 3–12, The Royal Society of Chemistry, London (http://afmb.cnrs-mrs.fr/CAZY).
2. Sinnott, M.L. (1990) Catalytic mechanisms of enzymatic glycosyl transfer. *Chem. Rev.* **90**, 1171–1202
3. Koshland, D.E., Jr. (1953) Stereochemistry and the mechanism of enzymatic reactions. *Biol. Rev.* **28**, 416–436
4. Johnson, L.N. and Phillips, D.C. (1965) Structure of some crystalline lysozyme-inhibitor complexes determined by X-ray analysis at 6 Angstrom resolution. *Nature* **206**, 761–763
5. Truscheit, E., Frommer, W., Junge, B., Müller, L., Schmidt, D.D., and Wingender, W. (1981) Chemistry and biochemistry of microbial α-glucosidase inhibitors. *Angew. Chem. Int. Ed. Engl.* **20**, 744–761
6. Cheetham, J.C., Artymiuk, P.J., and Phillips, D.C. (1992) Refinement of an enzyme complex with inhibitor bound at partial occupancy. Hen egg-white lysozyme and tri-N-acetylchitotriose at 1.75 Å resolution. *J. Mol. Biol.* **224**, 613–628
7. Takase, K., Matsumoto, T., Mizuno, H., and Yamane, K. (1992) Site-directed mutagenesis of active site residues in *Bacillus subtilis* α-amylase. *Biochim. Biophys. Acta* **1120**, 281–288
8. Qian, M., Haser, R., Buisson, G., Duee, E., and Payan, F. (1994) The active center of a mammalian α-amylase. Structure of the complex of a pancreatic α-amylase with a carbohydrate inhibitor refined to 2.2-Å resolution. *Biochemistry* **33**, 6284–6294
9. Divne, C., Ståhlberg, J., Reinikainen, T., Ruohonen, L., Pettersson, G., Knowles, J.K., Teeri, T.T., and Jones, T.A. (1994) The three-dimensional crystal structure of the catalytic core of cellobiohydrolase I from *Trichoderma reesei*. *Science* **265**, 524–528
10. Ståhlberg, J., Divne, C., Koivula, A., Piens, K., Claeyssens, M., Teeri, T.T., and Jones, T.A. (1996) Activity studies and crystal structures of catalytically deficient mutants of cellobiohydrolase I from *Trichoderma reesei*. *J. Mol. Biol.* **264**, 337–349
11. Divne, C., Ståhlberg, J., Teeri, T.T., and Jones, T.A. (1998) High-resolution crystal structures reveal how a cellulose chain is bound in the 50 Å long tunnel of cellobiohydrolase I from *Trichoderma reesei*. *J. Mol. Biol.* **275**, 309–325
12. Fujimoto, Z., Takase, K., Doui, N., Momma, M., Matsumoto, T., and Mizuno, H. (1998) Crystal structure of a catalytic-site mutant α-amylase from *Bacillus subtilis* complexed with maltopentaose. *J. Mol. Biol.* **277**, 393–407
13. Notenboom, V., Birsan, C., Nitz, M., Rose, D.R., Warren, R.A., and Withers, S.G. (1998) Insights into transition state stabilization of the β-1,4-glycosidase Cex by covalent intermediate accumulation in active site mutants. *Nat. Struct. Biol.* **5**, 812–818
14. Withers, S.G., Rupitz, K., and Street, I.P. (1988) 2-Deoxy-2-fluoro-D-glycosyl fluorides. A new class of specific mechanism-based glycosidase inhibitors. *J. Biol. Chem.* **263**, 7929–7932
15. Miao, S., Ziser, L., Aebersold, R., and Withers, S.G. (1994) Identification of glutamic acid 78 as the active site nucleophile in *Bacillus subtilis* xylanase using electrospray tandem mass spectrometry. *Biochemistry* **33**, 7027–7032
16. White, A., Tull, D., Johns, K., Withers, S.G., and Rose, D.R. (1996) Crystallographic observation of a covalent catalytic intermediate in a β-glycosidase. *Nature Struct. Biol.* **3**, 149–154
17. Davies, G.J., Mackenzie, L., Varrot, A., Dauter, M., Brzozowski, A.M., Schülein, M., and Withers, S.G. (1998) Snapshots along an enzymatic reaction coordinate: analysis of a retaining β-glycoside hydrolase. *Biochemistry* **37**, 11707–11713
18. Sidhu, G., Withers, S.G., Nguyen, N.T., McIntosh, L.P., Ziser, L., and Brayer, G.D. (1999) . Sugar ring distortion in the glycosyl-enzyme intermediate of a family G/11 xylanase. *Biochemistry* **38**, 5346–5354
19. Varrot, A., Schulein, M., and Davies, G.J. (2000) Insights into ligand-induced conformational change in Cel5A from *Bacillus agaradhaerens* revealed by a catalytically active crystal form. *J. Mol. Biol.* **297**, 819–828
20. Vocadlo, D.J., Davies, G.J., Laine, R., and Withers, S.G. (2001) Catalysis by hen egg-white lysozyme proceeds via a covalent intermediate. *Nature* **412**, 835–838
21. Ducros, V.M., Zechel, D.L., Murshudov, G.N., Gilbert, H.J., Szabó, L., Stoll, D., Withers, S.G, and Davies, G.J. (2002) Substrate distortion by a β-mannanase: snapshots of the Michaelis and covalent intermediate complexes suggest a $B_{2,5}$ conformation for the transition-state. *Angew. Chem. Int. Ed.* **41**, 2824–2827
22. Hövel, K., Shallom, D., Niefind, K., Belakhov, V., Shoham, G., Baasov, T., Shoham, Y., and Schomburg, D. (2003) Crystal structure and snapshots along the reaction pathway of a family 51 α-L-arabinofuranosidase. *EMBO J.* **22**, 4922–4932
23. Varrot, A and Davies, G.J. (2003) Direct experimental observation of the hydrogen-bonding network of a glycosidase along its reaction coordinate revealed by atomic resolution analyses of endoglucanase Cel5A. *Acta Crystallogr. Sect. D* **59**, 447–452
24. Amaya, M.F., Watts, A.G., Damager, I., Wehenkel, A., Nguyen, T., Buschiazzo, A., Paris, G., Frasch, A.C., Withers, S.G., and Alzari, P.M. (2004) Structural insights into the catalytic mechanism of *Trypanosoma cruzi trans*-sialidase. *Structure* **12**, 775–784
25. Vasella, A., Davies, G.J., and Böhm, M. (2002) Glycosidase mechanisms. *Curr. Opin. Chem. Biol.* **6**, 619–629

26. Money, V.A., Smith, N.L., Scaffidi, A., Stick, R.V., Gilbert, H.J., and Davies, G.J. (2006) Substrate distortion by a lichenase highlights the different conformational itineraries harnessed by related glycoside hydrolases. *Angew. Chem. Int. Ed.* **45**, 5136–5140
27. Biarnés, X., Nieto, J., Planas, A., and Rovira, C. (2006) Substrate distortion in the Michaelis complex of *Bacillus* 1,3-1,4-β-Glucanase. *J. Biol. Chem.* **281**, 1432–1441
28. Davies, G.J., Ducros, V.M., Varrot, A., and Zechel, D.L. (2003) Mapping the conformational itinerary of β-glycosidases by X-ray crystallography. *Biochem. Soc. Trans.* **31**, 523–527
29. Newstead, S.L., Potter, J.A., Wilson, J.C., Xu, G., Chien, C.H., Watts, A.G., Withers, S.G., and Taylor, G.L. (2008) The structure of *Clostridium perfringens* nani sialidase and its catalytic intermediates. *J. Biol. Chem.* **283**, 9080–9088
30. MacLeod, A.M., Lindhorst, T., Withers, S.G., and Warren, R.A. (1994) The acid/base catalyst in the exoglucanase/xylanase from *Cellulomonas fimi* is glutamic acid 127: evidence from detailed kinetic studies of mutants. *Biochemistry* **33**, 6371–6376
31. Zechel, D.L., Reid, S.P., Stoll, D., Nashiru, O., Warren, R.A., and Withers, S.G. (2003) Mechanism, mutagenesis, and chemical rescue of a β-mannosidase from *cellulomonas fimi*. *Biochemistry* **42**, 7195–7204
32. Kuno, A., Shimizu, D., Kaneko, S., Koyama, Y., Yoshida, S., Kobayashi, H., Hayashi, K., Taira, K., and Kusakabe, I. (1998) PCR cloning and expression of the F/10 family xylanase gene from *Streptomyces olivaceoviridis* E-86. *J. Ferment. Biotechnol.* **86**, 434–439
33. Kuno, A., Shimizu, D., Kaneko, S., Hasegawa, T., Gama, Y., Hayashi, K., Kusakabe, I., and Taira, K. (1999) Significant enhancement in the binding of *p*-nitrophenyl-β-D-xylobioside by the E128H mutant F/10 xylanase from *Streptomyces olivaceoviridis* E-86. *FEBS Lett.* **450**, 299–305
34. Kuno, A., Kaneko, S., Ohtsuki, H., Ito, S., Hasegawa, T., Taira, K., Kusakabe, I., and Hayashi, K. (2000) Novel sugar-binding specificity of the type XIII xylan-binding domain of a family F/10 xylanase from *Streptomyces olivaceoviridis* E-86. *FEBS Lett.* **482**, 231–236
35. Kaneko, S., Kuno, A., Fujimoto, Z., Shimizu, D., Machida, S., Go, M., Mizuno, H., Taira, K., Kusakabe, I., and Hayashi, K. (1999) An investigation of the nature and function of module 10 in a family F/10 xylanase FXYN of *Streptomyces olivaceoviridis* E-86 by module shuffling with the Cex of *Cellulomonas fimi* and by site-directed mutagenesis. *FEBS Lett.* **460**, 61–66
36. Kaneko, S., Iwamatsu, S., Kuno, A., Fujimoto, Z., Sato, Y., Yura, K., Go, M., Mizuno, H., Taira, K., Hasegawa, T., Kusakabe, I., and Hayashi, K. (2000) Module shuffling of a family F/10 xylanase: replacement of modules M4 and M5 of the FXYN of *Streptomyces olivaceoviridis* E-86 with those of the Cex of *Cellulomonas fimi*. *Protein Eng.* **13**, 873–879
37. Kaneko, S., Ichinose, H., Fujimoto, Z., Kuno, A., Yura, K., Go, M., Mizuno, H., Taira, K., Kusakabe, I., and Kobayashi, H. (2004) Structure and function of a family 10 β-xylanase chimera of *Streptomyces olivaceoviridis* E-86 FXYN and *Cellulomonas fimi* Cex. *J. Biol. Chem.* **279**, 26619–26626
38. Fujimoto, Z., Kuno, A., Kaneko, S., Yoshida, S., Kobayashi, H., Kusakabe, I., and Mizuno, H. (2000) Crystal structure of *Streptomyces olivaceoviridis* E-86 β-xylanase containing xylan-binding domain. *J. Mol. Biol.* **300**, 575–585
39. Fujimoto, Z., Kuno, A., Kaneko, S., Kobayashi, H., Kusakabe, I., and Mizuno, H. (2002) Crystal structures of the sugar complexes of *Streptomyces olivaceoviridis* E-86 xylanase: sugar binding structure of the family 13 carbohydrate binding module. *J. Mol. Biol.* **316**, 65–78
40. Fujimoto, Z., Kaneko, S., Kuno, A., Kobayashi, H., Kusakabe, I., and Mizuno, H. (2004) Crystal structures of decorated xylooligosaccharides bound to a family 10 xylanase from *Streptomyces olivaceoviridis* E-86. *J. Biol. Chem.* **279**, 9606–9614
41. Kaneko, S., Kitaoka, M., Kuno, A., and Hayashi, K. (2000) Syntheses of 4-methylumbelliferyl-β-D-xylobioside and 5-bromo-3-indolyl-β-D-xylobioside for sensitive detection of xylanase activity on agar plates. *Biosci. Bioeng. Biochem.* **64**, 741–745
42. Miyazaki, K. and Arnold, F.H. (1999) Exploring nonnatural evolutionary pathways by saturation mutagenesis: rapid improvement of protein function. *J. Mol. Evol* **49**, 716–720
43. Takeo, K., Ohguchi, Y., Hasegawa, R., and Kitamura, S. (1995) Synthesis of 2- and 4-nitrophenyl β-glycosides of β-(1→4)-D-xylo-oligosaccharides of dp 2–4. *Carbohydrate Res.* **277**, 231–244
44. Otwinowski, Z. and Minor, W. (1997) Processing of X-ray diffraction data collected in oscillation mode. *Methods Enzymol.* **276**, 307–326
45. Brünger, A.T., Adams, P.D., Clore, G.M., DeLano, W.L., Gros, P., Grosse-Kunstleve, R.W., Jiang, J. S., Kuszewski, J., Nilges, M., Pannu, N.S., Read, R.J., Rice, L.M., Simonson, T., and Warren, G.L. (1998) Crystallography and NMR system: a new software suite for macromolecular structure determination. *Acta Crystallogr. Sect. D* **54**, 905–921
46. Banait, N.S. and Jencks, W.P. (1991) Reactions of anionic nucleophiles with α-D-glucopyranosyl fluoride in aqueous solution through a concerted, A_ND_N (S_N2) mechanism. *J. Am. Chem. Soc.* **113**, 7951–7958
47. Uitdehaag, J.C., Mosi, R., Kalk, K.H., van der Veen, B.A., Dijkhuizen, L., Withers, S.G., and Dijkstra, B.W. (1999) X-ray structures along the reaction pathway of cyclodextrin glycosyltransferase elucidate catalysis in the α-amylase family. *Nat. Struct. Biol.* **6**, 432–436
48. Sandgren, M., Berglund, G.I., Shaw, A., Ståhlberg, J., Kenne, L., Desmet, T., and Mitchinson, C. (2004) Crystal complex structures reveal how substrate is bound in the −4 to the +2 binding sites of *Humicola grisea* Cel12A. *J. Mol. Biol.* **342**, 1505–1517
49. Sulzenbacher, G., Driguez, H., Henrissat, B., Schülein, M., and Davies, G.J. (1996) Structure of the *Fusarium oxysporum* endoglucanase I with a nonhydrolyzable substrate analogue: substrate distortion gives rise to the preferred axial orientation for the leaving group. *Biochemistry* **35**, 15280–15287
50. Gorenstein, D.G. and Taira, K. (1984) Stereoelectronic control in peptide bond formation. Ab initio calculations and speculations on the mechanism of action of serine proteases. *Biophys. J.* **46**, 749–761
51. Deslongchamps, P. (1993) Intramolecular strategies and stereoelectronic effects. Glycosides hydrolysis revisited. *Pure Appl. Chem.* **65**, 1161–1178
52. Jencks, W.P. (1975) Binding energy, specificity, and enzymic catalysis: the circe effect. *Adv. Enzymol. Relat. Areas Mol. Biol.* **43**, 219–410
53. Cleland, W.W. and Kreevoy, M.M. (1994) Low-barrier hydrogen bonds and enzymic catalysis. *Science* **264**, 1887–1890
54. Frey, P.A., Whitt, S.A., and Tobin, J.B. (1994) A low-barrier hydrogen bond in the catalytic triad of serine proteases. *Science* **264**, 1927–1930